Journal of
Marine Science and Engineering

MDPI

Article

Applying Neural Networks to Predict Offshore Platform Dynamics

Nikolas Martzikos *, Carlo Ruzzo, Giovanni Malara, Vincenzo Fiamma and Felice Arena

Natural Ocean Engineering Laboratory (NOEL), "Mediterranea" University of Reggio Calabria, Loc. Feo di Vito, 89122 Reggio Calabria, Italy; carlo.ruzzo@unirc.it (C.R.); giovanni.malara@unirc.it (G.M.); vincenzo.fiamma@unirc.it (V.F.); arena@unirc.it (F.A.)
* Correspondence: nikolas.martzikos@unirc.it

Abstract: Integrating renewable energy sources with aquaculture systems on floating multi-use platforms presents an innovative approach to developing sustainable and resilient offshore infrastructure, utilizing the ocean's considerable potential. From March 2021 to January 2022, a 1:15-scale prototype was tested in Reggio Calabria, Italy, which gave crucial insights into how these structures behave under different wave conditions. This study investigates the application of Artificial Neural Networks (ANNs) to predict changes in mooring loads, particularly at key points of the structure. By analyzing metocean data, several ANN models and optimization techniques were evaluated to identify the most accurate predictive model. With a Normalized Root Mean Square Error (NRMSE) of 1.7–4.7%, the results show how ANNs can effectively predict offshore platform dynamics. This research highlights the potential of machine learning in developing and managing sustainable ocean systems, setting the stage for future advancements in data-driven marine resource management.

Keywords: artificial neural networks; offshore platforms; aquaculture platforms; mooring loads; renewable energy

Citation: Martzikos, N.; Ruzzo, C.; Malara, G.; Fiamma, V.; Arena, F. Applying Neural Networks to Predict Offshore Platform Dynamics. *J. Mar. Sci. Eng.* **2024**, *12*, 2001. https://doi.org/10.3390/jmse12112001

Academic Editors: Zhenhua Ma and Jianguang Qin

Received: 27 September 2024
Revised: 5 November 2024
Accepted: 5 November 2024
Published: 7 November 2024

1. Introduction

The transition to renewable energy is crucial for addressing the interconnected challenges of climate change, energy security, and sustainable development. Offshore wind energy, with its higher and more consistent wind speeds compared to land-based alternatives, represents a substantial advancement in reducing carbon emissions [1]. Offshore wind farms take advantage of stronger sea winds, producing electricity for longer periods and avoiding common issues like noise pollution that often arise with onshore wind [2]. As the global population continues to grow, the demand for sustainable energy intensifies, driving innovation in areas like Marine Renewable Energy (MRE) and aquaculture [3]. These industries play a crucial role in addressing energy demands while also contributing to broader socio-economic goals. The concept of "Blue Growth" highlights the sustainable use of ocean resources, with developments like multi-use offshore platforms that combine energy production with other functions, making them more cost-effective and operationally efficient [3,4]. This integrated approach to ocean space addresses immediate energy needs while establishing a foundation for future technological and environmental balance, essential for long-term sustainability.

As the focus on renewable energy grows, there is an increasing interest in the structural dynamics of offshore platforms [5,6]. This research is essential to ensure the reliability and efficiency of these structures, especially in harsh marine environments, as they take on multiple roles, from energy generation to aquaculture. Studies looking into the dynamic responses of these platforms under different environmental conditions are particularly important [7,8]. They help to better understand the limits and capabilities of these structures, leading to improvements in design and technology, especially in mooring systems, which

are vital for sustainable development [9]. Moreover, advancements in related areas, such as structural health monitoring and electrical transmission, particularly through sensor applications in offshore cables and multi-terminal high-voltage networks, further highlight the growing significance of offshore infrastructure research [10–13].

The use of Artificial Neural Networks (ANNs) and Machine Learning (ML) techniques in marine engineering has been highlighted by various studies, including applications in the optimization of marine structures [14]. More recently, these techniques have been applied to analyze the dynamic behaviour of multi-use offshore platforms and manage mooring loads. While ANNs are the focus of this study, other methods, such as genetic algorithms, support vector machines, and hybrid artificial intelligence (AI) models, have also shown promise in similar applications [15–19]. These computational tools allow for accurate modelling and the control of complex structures facing varying environmental forces, improving the safety and efficiency of renewable energy platforms. For instance, combining Floating Offshore Wind Turbines (FOWTs) with Oscillating Water Columns (OWCs) helps optimize energy absorption and reduce dynamic responses [20]. Neural network controllers have also been applied to stabilize platforms against wave impacts, showing significant improvements over traditional control methods [21].

There has also been progress in neural simulators for mooring system design, which use historical environmental data and machine learning to improve design accuracy and efficiency [22]. This approach is complemented by using Bayesian networks to enhance the reliability analysis of mooring systems [23], and machine learning models to predict significant wave heights, which is crucial for the operation and maintenance of offshore energy farms [24].

These new approaches enhance the predictive capabilities of dynamic models and support the development of adaptive control systems, improving platform stability and efficiency in variable conditions. Together, these studies underline the key role of machine learning and neural network technologies in advancing the design and functionality of offshore renewable energy systems, promising a more resilient and efficient future for multi-functional marine structures.

The objective of this article is to assess the reliability of an ANN-based algorithm for predicting the mooring load on a multi-purpose floating platform exposed to random sea waves. For achieving this objective, field data collected during an experimental campaign in a natural basin are used. The following sections will provide a description of the experimental activity and of the ANN architecture (Section 2), the results and discussion with the limits of the proposed ANN-based procedure (Section 3), and concluding remarks (Section 4).

2. Materials and Methods

The field experiment took place at the Natural Ocean Engineering Laboratory (NOEL) at the Mediterranean University of Reggio Calabria, Italy. NOEL is known for allowing real-time monitoring of natural sea conditions, which made it an ideal setting for this study. Small, wind-driven sea states were observed with significant wave heights ranging from 0.20 m to 0.80 m and peak wave periods between 2.0 and 3.6 s, with characteristics similar to JONSWAP spectra. The experiment ran from March 2021 to January 2022, with the most focused data collection occurring between May and July 2021.

During the experiment, a 1:15-scaled prototype of a floating multi-use platform (Figure 1) was equipped with an array of sensors. The platform was designed to combine an automated offshore aquaculture plant with wave and wind energy harvesting technologies. It was made up of a rectangular-shaped, steel, semi-submersible hull with a T-shaped cross section. A scaled 10-MW wind turbine [25] and an array of U-shaped OWC [26] wave energy converters were placed in the front side of the hull. The aquaculture cages were instead hosted in the internal moonpool, to be protected from the incoming waves. The scope of the experiment was to investigate the complex dynamic of the platform, considering various dynamic couplings, including those between the floater, the mooring system,

the wind and wave energy converters, the internal moonpool, and the cages. Extensive description of the activities can be found in [4,27].

Figure 1. Photo of BGF platform installed at NOEL.

In this paper, a sample of 4458 data records is considered, collected between 26 May and 6 July 2021. Each record is 10 min long and has a sampling frequency of 10 Hz, compatible with the site wave properties [28] and with the dynamic characteristics of the platform model. In more detail, previous experimental identification analyses (see, e.g., [4]) had shown that its natural frequencies lay approximately in the range of 0.12–0.15 rad/s for the horizontal motions (surge, sway, yaw) and 1.35–1.62 rad/s for the vertical motions (heave, roll, pitch). Specifically, the following sensors were used in this analysis:

- Load cells were placed at the fairleads of three out of four catenary mooring lines (i.e., South-East (SE), South-West (SW), and North-East (NE) corners) of the structure to measure forces. AEP CTS1025TC25 load cells were used, with a nominal load of 5 tons. These sensors have a combined error, non-repeatability, and creep at nominal load of over 20–30 min, all under $\pm 0.025\%$. Sensitivity tolerance is also within $\pm 0.1\%$.
- Pressure transducers were used to measure the wave head of pressure in an undisturbed field. An STS ATM.1ST model was used, which operates in a range of 0.0–0.7 bar, making it suitable for both normal and extreme wave conditions at NOEL. The sensor's measurement uncertainty is within $\pm 0.25\%$.
- Ultrasonic probes were used to measure the free-surface displacement. The FAE IRU-2003 model provided direct measurements of the distance between the sensor and the wave surface, which allowed for the determination of the wave profile. This sensor has a default measurement range of 0.30–7.62 m, perfectly suited to the conditions at NOEL.
- A Gill WindSonic M 2-D ultrasonic anemometer (Gill Instruments Limited, Lymington, United Kingdom) was used to measure the wind velocity and direction in the horizontal plane. The wind measurements were acquired independently from the wave ones,

at a reduced sampling frequency of 4 Hz, consistently with sensor capability and local wind dynamic properties.

It is worth noting that the pressure gauges and ultrasonic probes were used to quantify sea state characteristics in undisturbed conditions, i.e., at a sufficient distance from the structure to assume as negligible its diffraction/radiation effects. To achieve this, they were installed far from the BGF structure on two ballasted vertical piles (Figure 2), at water depths of 1.90 m and 3.70 m, respectively, and were spaced 2.75 m apart. This arrangement followed the method developed by Boccotti et al. [29] to estimate the statistical and spectral characteristics of the sea states. Also, the wind was measured in the undisturbed field.

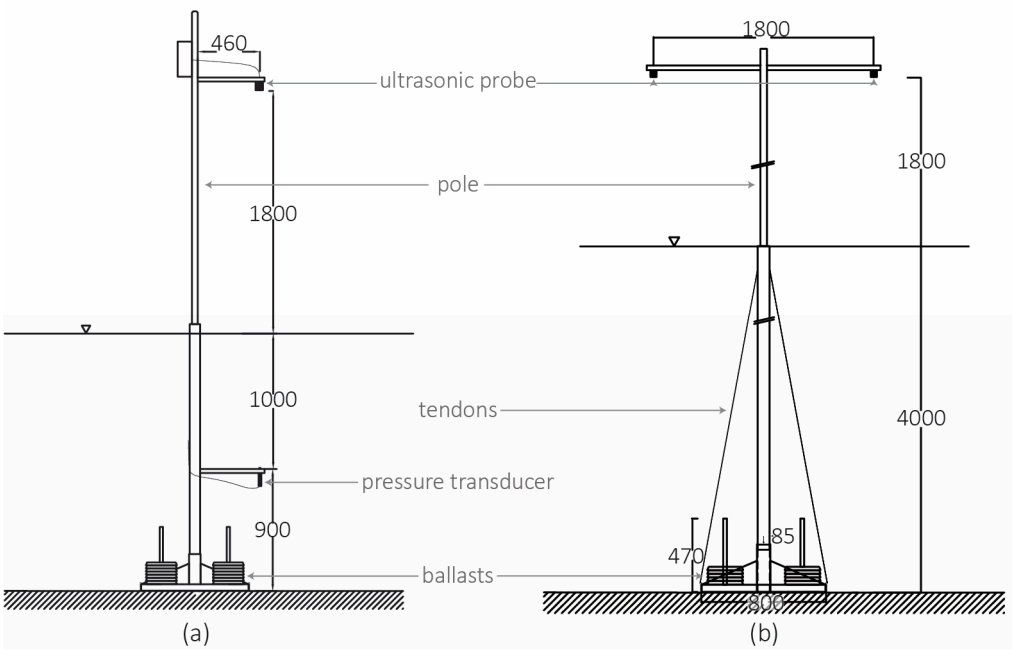

Figure 2. Geometrical characteristics of ballasted vertical piles installed nearshore (**a**) and offshore (**b**). All lengths are provided in millimetres [mm].

These data offered an in-depth view of how the platform interacts with its environment, highlighting the complex relationship between its structural dynamics and the wave climate. This understanding is essential for improving the design and operational protocols of such innovative marine multi-use structures.

In this study, ANNs were trained using a comprehensive set of variables that included wave climate factors, as well as parameters representing the structural loads. The list of the variables used is reported in Table 1.

The choice of the mooring loads (SW, SE, and NE cells) was driven by data availability, as the NW cell had a disconnection period during the experiment. However, the data that were used are deemed sufficient to preliminarily investigate the variability and peaks in the mooring loads. The choice of the wave parameters was aimed to completely characterize the wave properties, including magnitude, wave energy distribution in the frequency domain, and direction. In particular, since bimodal spectra cannot be fully characterized by synthetic variables such as mean and peak wave period, the ratio between wind-generated (periods from $T_1 = 2\pi/\omega_1 = 3.0$ s to $T_2 = 2\pi/\omega_2 = 1.0$ s) and swell (periods from $T_3 = 2\pi/\omega_3 = 11.9$ s to T_1) spectral components (areas) has been introduced and is defined as

$$Ratio_{w,swell} = \frac{\int_{\omega_1}^{\omega_2} S(\omega)d\omega}{\int_{\omega_3}^{\omega_1} S(\omega)d\omega} \quad (1)$$

where $S(\omega)$ is the wave frequency spectrum and ω the frequency.

Table 1. Variables used for training the ANNs, with corresponding symbols, sensors, and units; d represents water depth.

	Variable	Symbol	Sensor	Units
Mooring loads	Load at the south-west fairlead	T_{SW}	Load cells	[N]
	Load at the south-east fairlead	T_{SE}		
	Load at the north-east fairlead	T_{NE}		
Surface wave	Significant height	Hs (d = 3.70 m) Hs_{coast} (d = 1.90 m)	Ultrasonic probes	[m]
	Peak period	Tp_1 (d = 1.90 m—left) Tp_2 (d = 1.90 m—right)		[s]
	Wind-generated/swell spectral area ratio	$Ratio_{w,swell}$		[-]
	Mean zero-up-crossing period	Tz (d = 3.70 m) Tz_{coast} (d = 1.90 m)		[s]
	Mean propagation direction	$\overline{\theta}$ (d = 3.70 m) $\overline{\theta}_{coast}$ (d = 1.90 m)		[rad]
Head of pressure wave	Peak period	Tp_{Ph2} (d = 1.90 m)	Pressure transducers	[s]
	Significant height	$Hs_{Phcoast}$ (d = 1.90 m)		[m]
	Mean zero-up-crossing period	$Tz_{Phcoast}$ (d = 1.90 m)		[s]
Wind	Mean direction	$\overline{Dir}_w$	Anemometer	[rad]
	Mean velocity	$\overline{u}_w$		[m/s]

The methodology that was employed focused on developing and refining ANNs to predict the dynamic response of the floating multi-use offshore platform. Using the dataset collected from the field experiment, this approach involved optimizing the ANN model structure and investigating its predictive accuracy under various environmental conditions.

To build the final model, ANNs were developed and validated following a systematic process:

- Data preparation: a cleaning process of the data was applied to remove any inconsistencies and gaps, ensuring the dataset was reliable for further analysis.
- Dataset division: The cleaned dataset was then split into training and test sets, using an 80–20% ratio. This split is commonly used in the field [30] to allow the model to be evaluated on unseen data, ensuring its performance holds up in real-world scenarios. From the training set, an additional 10% was further split off to serve as a validation set.
- ANN architecture selection: different feed-forward Deep Neural Networks (DNNs) were explored to find the best balance between complexity and learning efficiency.
- Robustness enhancement: to make the models more robust and reduce uncertainty, 10-fold cross-validation was employed, with multiple realizations run for each configuration.
- Training data length optimization: the length of the training data was adjusted to ensure there was enough information for the model to learn from without overloading it.
- Hyperparameter tuning: the model's hyperparameters were carefully adjusted to improve its learning efficiency and overall predictive accuracy.
- Input variable assessment: the input variables were thoroughly evaluated to determine their significance, ensuring that only the most relevant factors were used in the ANN models.

The data cleaning process involved discarding missing values to ensure only complete data were used, detecting and removing outliers above the 99th percentile, and normalizing the data. Most variables were scaled to the range $[-1, 1]$ through min–max normalization, while directional variables (i.e., $\overline{\theta}$, $\overline{\theta}_{coast}$) were transformed using the trigonometric functions (i.e., $sin\overline{\theta}$, $cos\overline{\theta}$, $sin\overline{\theta}_{coast}$, $cos\overline{\theta}_{coast}$) to account for their cyclical nature.

In this step, TensorFlow [31] in Python was used to build and train the neural networks. The architectures varied in the following key parameters:

- Input layer: 17 features based on the training data.

- Hidden layers: the number of hidden layers was dynamically adjusted between 1 and 5, there being a DNN when more than one layer was used.
- Units per layer: each hidden layer could have between 32 and 512 units, with the specific number of units per layer being determined through hyperparameter tuning.
- Activation functions: both 'ReLU' and 'tanh' were explored as activation functions, with 'ReLU' introducing non-linearity and 'tanh' providing bounded activation.
- Learning rate: the Adam optimizer was used with a learning rate dynamically tuned between 1×10^{-5} and 1×10^{-2}.
- Output: Each approach predicted three load cell-related features for the directions SE, SW, and NE. The first approach focused on predicting the maximum, while the second approach predicted the standard deviation of the load cell ($max(T_{SE})$, $max(T_{SW})$, $max(T_{NE})$ and $\sigma(T_{SE})$, $\sigma(T_{SW})$, $\sigma(T_{NE})$).

The hyperparameter optimization was conducted using the RandomSearch tuner from TensorFlow's Keras Tuner library. RandomSearch performed an initial broad search, minimizing the validation mean squared error across 10 trials, with each trial executed twice. The best hyperparameters identified during this process were then used to build and train the final model on the training dataset for 50 epochs. The model's performance was subsequently validated on a separate dataset and evaluated on the test dataset using metrics such as test loss, Root Mean Square Error (RMSE), and Normalized Root Mean Square Error (NRMSE). In addition to RandomSearch, a Bayesian optimization and Hyperband methods [32,33] were utilized. Bayesian optimization fine-tuned high-performing parameters by constructing a probabilistic model based on previous results, while Hyperband expedited the process by adaptively allocating resources and using early stopping to focus on the best-performing models. The optimization process was conducted in three stages across three different ANNs: starting with a grid search, followed by Bayesian optimization, and finally, the introduction of Hyperband. This sequential approach allowed us to compare RMSEs and ultimately select the best-performing model.

The RMSE and NRMSE metrics were calculated between the predicted $\left(y_{predicted}\right)$ and actual $\left(y_{actual}\right)$ values using the following formulas, where n is the number of observations, and y_{max} and y_{min} represent the maximum and minimum values in the dataset, respectively:

$$RMSE = \sqrt{\frac{1}{n}\sum_{t=1}^{n}\left(y_{t,predicted} - y_{t,actual}\right)^2}, \tag{2}$$

$$NRMSE = \frac{RMSE}{y_{max} - y_{min}} \cdot 100 \tag{3}$$

To rigorously determine the impact of each input variable on the predictions made by the ANNs, the permutation importance method [34,35] was used. This approach is crucial for identifying the most influential features in the model, ensuring that only the most relevant predictors are included. The method works by shuffling the values of each feature while keeping the target values fixed, then measuring the decrease in model performance. This decrease indicates the feature's importance. The permutation process was repeated 10 times to account for random variations and ensure robustness. The importance of each feature was quantified by the mean decrease in performance, resulting in unitless scores that reflect the relative importance of each predictor. In this way, the methodology enhances both the transparency of the predictive models and the optimization of the network architecture and hyperparameter settings.

The standard deviation ($\sigma(T_{SE})$, $\sigma(T_{SW})$, $\sigma(T_{NE})$) and maximum ($max(T_{SE})$, $max(T_{SW})$, $max(T_{NE})$) of load cell values for each record were selected as the primary output variables for the ANNs. The standard deviation provides insights into the variability and stability of the structure, while the maximum values highlight the peak load that the structure can withstand. Two separate iterations of the ANNs were conducted, one focused on predicting maximum values and the other on standard deviations. This dual approach

captures different aspects of the mooring load dynamics under varying metocean conditions, deepening the understanding of the relationship between environmental forces and structural responses. In Figure 3, both output variables, as recorded before any processing, are represented across the sampling period used in this work, illustrating the variations in maximum and standard deviation load values over time.

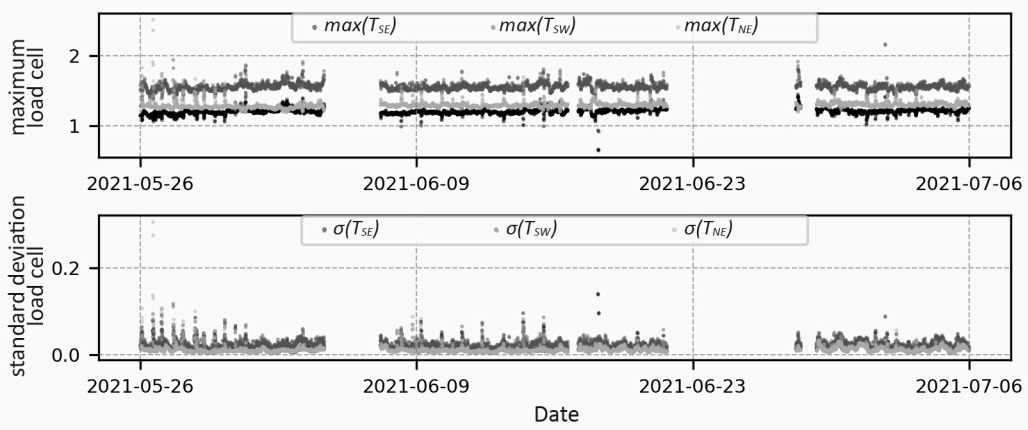

Figure 3. Maximum and standard deviation load cell values over sampling period.

3. Results and Discussion

After applying ANNs to predict both the maximum and standard deviation of load cell values in the SW, SE, and NW directions, the NRMSE for standard deviation was observed as higher compared to that of the maximum values (Table 2). This higher NRMSE indicates a greater difficulty in accurately predicting variability, which reflects the inherently stochastic nature of marine environments more than peak loads. Given the importance of standard deviation in capturing the variability and uncertainties in these conditions, this work focused on its prediction.

Table 2. The errors (RMSE, NRMSE) of the predicted maximum and standard deviation of load cell values through the ANNs.

	$max(T_{SE})$	$max(T_{SW})$	$max(T_{NE})$	$\sigma(T_{SE})$	$\sigma(T_{SW})$	$\sigma(T_{NE})$
RMSE	0.031	0.043	0.051	0.008	0.008	0.010
NRMSE%	3.776	5.307	3.865	6.016	7.098	3.467

Improving the accuracy of $\sigma(T_{SE})$, $\sigma(T_{SW})$, $\sigma(T_{NE})$ predictions is a more technically demanding but highly valuable task. This approach expands modelling capabilities and enhances the structural resilience, enabling better adaptation to variable loads. Prioritizing this focus is expected to significantly improve the reliability and predictive power of the ANNs, which is especially important for dynamic and complex environments where understanding variability is key to ensuring safety and optimizing performance.

To improve the predictive accuracy of the ANNs, a comprehensive analysis of input variable importance was conducted, which revealed several variables with minimal impact on model predictability (Figure 4). The feature importance was evaluated using the permutation importance method [36] from Python's Scikit-learn library [37]. This method measures the impact of each feature by calculating the increase in the model's error when the values of the feature are randomly shuffled. The importance scores reflect the corresponding changes in the performance of the model, with higher scores indicating features that have a greater influence on the predictions. As a result, variables related to the mean wave direction at both the available water depths ($cos_{\overline{\theta}_{coast}}, sin_{\overline{\theta}_{coast}}, cos_{\overline{\theta}}, sin_{\overline{\theta}}$) and to the mean wind direction ($\sigma(Dir_{\overline{W}})$) were excluded to streamline the model, reducing its complexity and enhancing computational efficiency. This exclusion was based on current

findings, though additional variables may be revised or excluded in future iterations as part of ongoing optimizations.

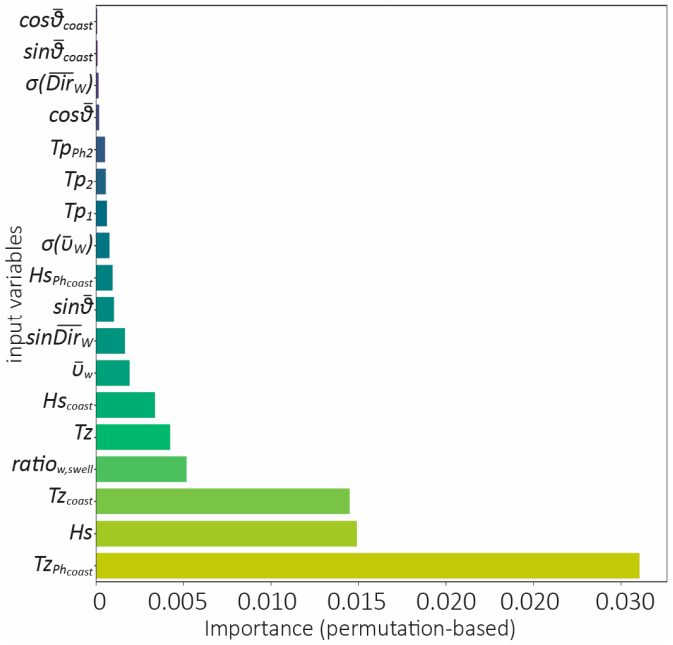

Figure 4. Permutation-based feature importance analysis of input variables.

To evaluate the impact of this refinement, the RMSE and NRMSE metrics before and after the variable exclusions were compared. The results, shown in Figure 5 along with normalized values, indicate minimal differences in performance metrics post-exclusion. This confirms that the streamlined model maintains its predictive accuracy while operating with reduced input complexity. These findings suggest that excluding these variables effectively simplifies the model without compromising its predictive capability, thereby validating this approach to improve model performance by focusing on more impactful variables.

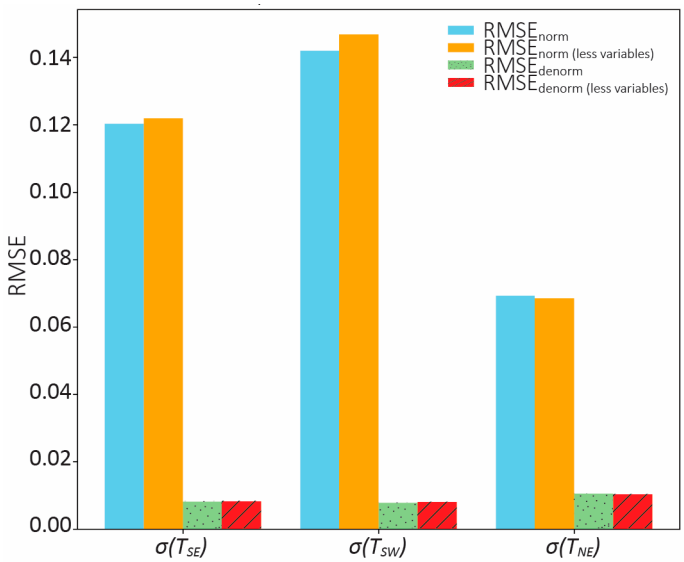

Figure 5. Comparative analysis of RMSE for normalized and denormalized predictions before and after skipping less important input variables.

The model was further optimized using both Bayesian optimization and Hyperband techniques in TensorFlow, with a focus on fine-tuning the hyperparameters to improve predictive accuracy. As shown in Table 3, the effectiveness of both optimization strategies was assessed using RMSE and NRMSE values across the three directions (SE, SW, NE). Bayesian optimization generally achieved slightly lower RMSE and NRMSE values compared to the Hyperband approach. In particular, the SE and SW directions showed consistently lower errors with Bayesian optimization, indicating a more accurate model fit. The stability of the Bayesian approach was further validated through 10-fold cross-validation, confirming its robustness across different data subsets. As a result, the ANN model refined using Bayesian optimization was selected for final implementation due to its better performance and reliability in predicting the standard deviation of load values.

Table 3. The errors (RMSE, NRMSE) of the predicted standard deviation loads through the ANNs.

		$\sigma(T_{SE})$	$\sigma(T_{SW})$	$\sigma(T_{NE})$
RMSE	Bayesian	0.007	0.007	0.010
	Hyperband	0.008	0.007	0.009
NRMSE (%)	Bayesian	5.416	6.518	3.210
	Hyperband	5.795	6.570	2.898

The optimal ANN was used to make the final predictions of $\sigma(T_{SE})$, $\sigma(T_{SW})$, and $\sigma(T_{NE})$. Figure 6 shows a comparison between the actual and predicted standard deviations for a randomly selected test dataset, demonstrating a close alignment between the two.

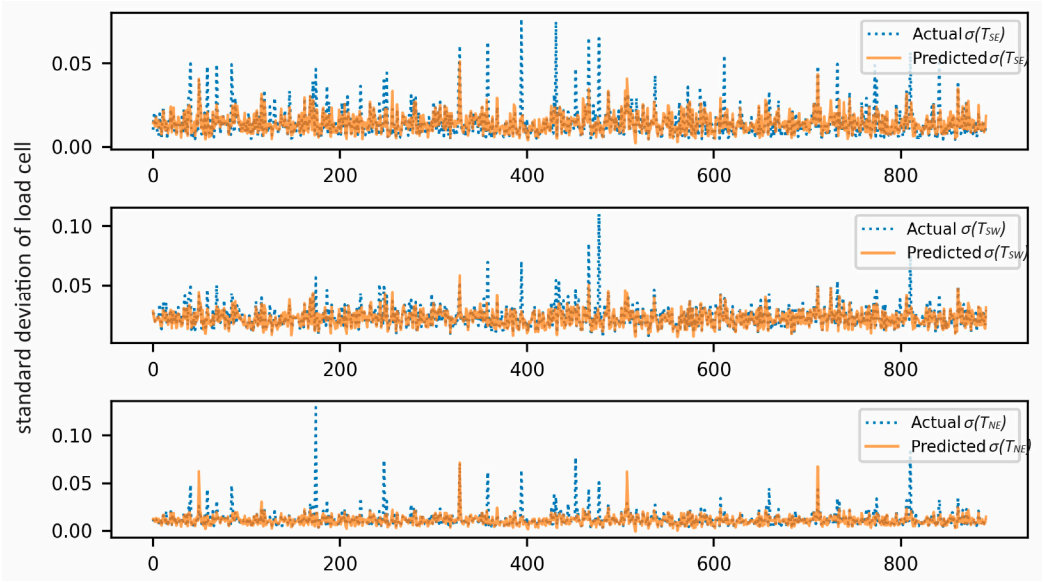

Figure 6. Comparison of actual vs. predicted values through final ANN using Bayesian optimization.

However, spikes detected in Figure 6 revealed significant differences between the predicted and actual values, leading to the consideration that discarding outliers above the 99th percentile might be beneficial. Further investigation identified that these outliers were caused by current-related phenomena occurring at the NOEL site, which are sporadic and not representative of significant platform dynamics. These phenomena were not consistently measured and do not reflect the platform's typical behaviour.

By applying this threshold, only 79 values were discarded, representing less than 1% of the dataset, without compromising the variability in the standard deviation. The removal of these extreme values improved the model's performance by reducing the influence of unrepresentative spikes. Following this adjustment, the final ANN was retrained using Bayesian optimization, and its accuracy was evaluated based on the new predictions

(Figure 7). The RMSE and NRMSE values, shown in Table 4, indicate improved model performance.

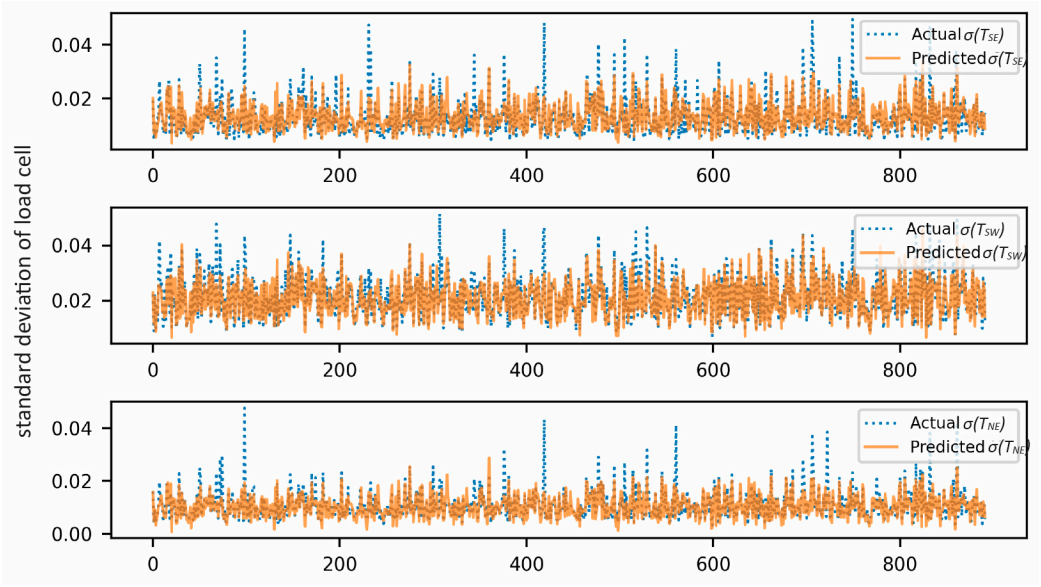

Figure 7. Comparison of actual vs. predicted values through final ANN using Bayesian optimization after discarding outliers above 99th percentile.

Table 4. The errors (RMSE, NRMSE) of the predicted standard deviation loads through the final ANN using Bayesian optimization after discarding the outliers.

	$\sigma(T_{SE})$	$\sigma(T_{SW})$	$\sigma(T_{NE})$
RMSE	0.006	0.005	0.005
NRMSE (%)	4.441	4.720	1.767

Further validation is presented in Figure 8, where a scatterplot between the predicted and actual standard deviations of load cells demonstrates a strong correlation, particularly in the SE and SW directions. This is evidenced by the close alignment of data points along the diagonal line, which indicates that the model's predictions are highly accurate. Although the NE direction exhibits slightly more variability, the overall alignment of points highlights the ANN's high predictive accuracy and efficiency across different directions.

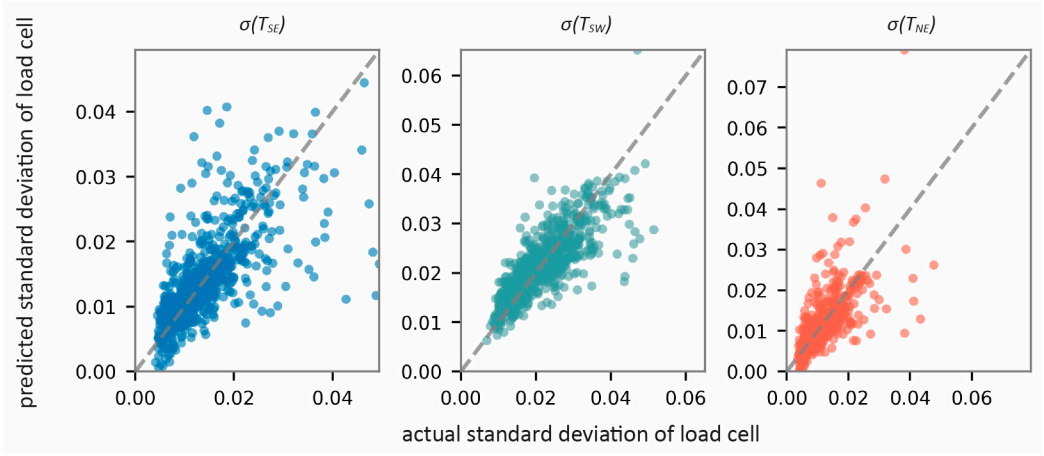

Figure 8. Comparison of predicted vs. actual standard deviation of load cells for SE, SW, and NE directions.

The residual plots in Figure 9 illustrate the difference between the predicted and actual standard deviations of load cells across the SE, SW, and NE directions. For SE, a clear negative monotonic trend is observed, where the error tends to increase with higher actual standard deviation values, indicating the model under-predicts for larger load values in this direction. SW shows a similar but less pronounced trend, while NE exhibits more variability, with residuals spread more widely compared to other directions, and without a clear pattern. This variability could suggest areas for further model refinement. Fine-tuning the hyperparameters or incorporating additional training data for higher load cases could enhance future model performance.

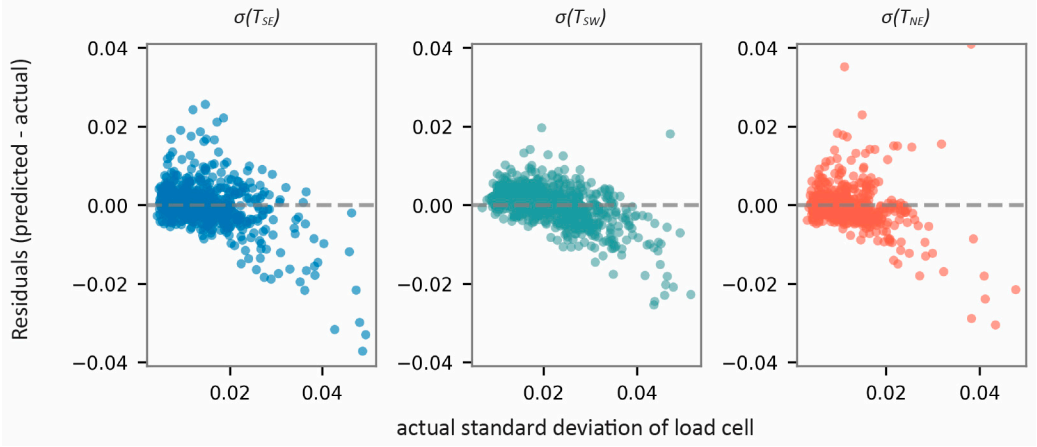

Figure 9. Residual plot showing difference between predicted and actual standard deviation of load cells for SE, SW, and NE directions.

To provide an additional layer of validation for the model's accuracy and consistency, the error distribution plot was examined. Figure 10 illustrates the spread of prediction errors across the SE, SW, and NE directions. In all three directions, the distributions are tightly centred around zero, indicating that the model does not exhibit significant bias in over- or under-predicting the values. The distributions appear approximately symmetric and normally distributed, though the slight negative trend in SE residuals observed in Figure 8 is less obvious here. The error spread, typically ranging between −0.04 and 0.04, indicates that the model's predictions are generally close to the actual values. However, minor variations in the spread may suggest that the model performs slightly differently depending on the direction, with NE exhibiting a narrower error distribution and a slightly higher peak frequency.

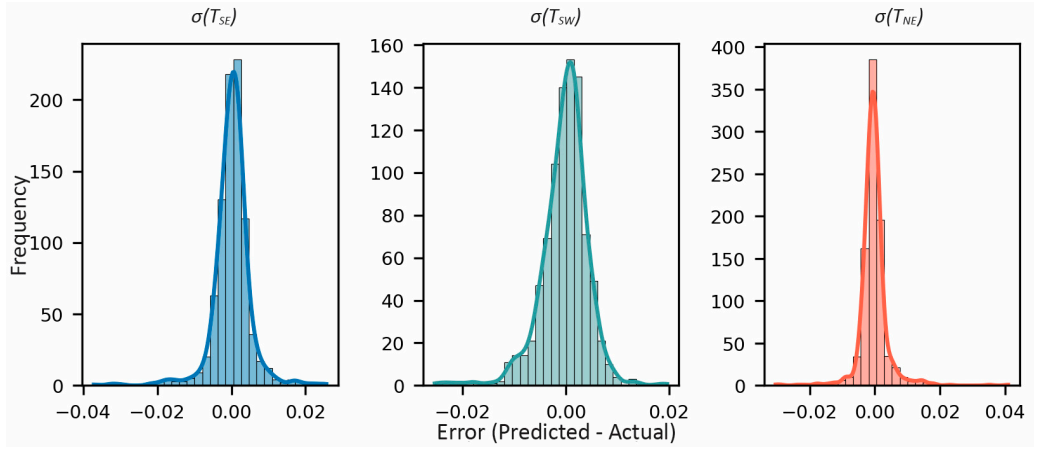

Figure 10. Error distribution of predicted standard deviation of load cells in SE, SW, and NE directions.

To further assess the model's robustness across varying environmental conditions, the relationship between prediction errors and significant wave heights was analyzed. As shown in Figure 11, the data do not suggest a strong correlation between higher prediction errors and larger wave heights, indicating consistent model performance across the range of conditions tested. The distribution of errors across the SE, SW, and NE directions appears relatively symmetrical, suggesting that the model does not exhibit a systematic bias toward overestimation or underestimation. This uniformity is encouraging, as it suggests the model's predictions are unbiased overall. However, although the model maintains consistent performance, some outliers are present across a range of wave heights. These outliers suggest that further refinements may be needed to improve predictive precision in certain cases, although they do not seem to be linked to extreme wave conditions.

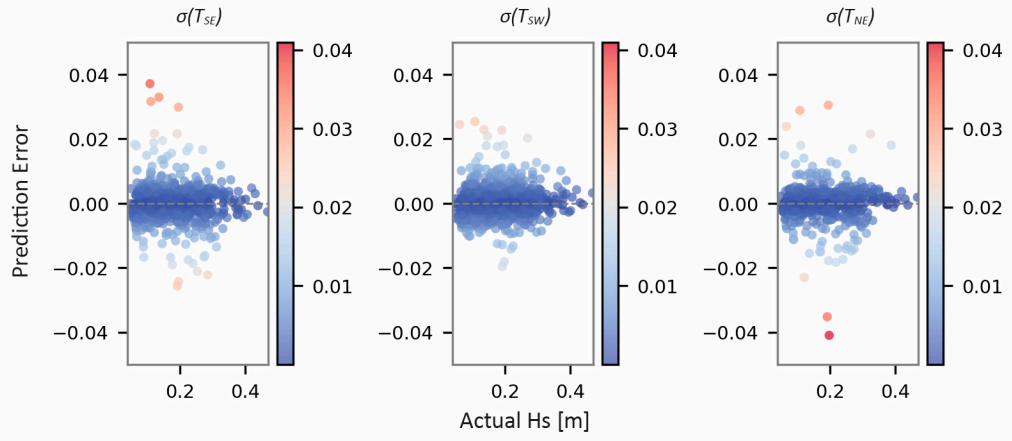

Figure 11. Analysis of prediction errors relative to significant wave height.

4. Conclusions

In conclusion, this study proposed the application of ANNs for the prediction of the mooring loads of a multi-purpose floating platform and demonstrated its effectiveness based on the field data collected at the Natural Ocean Engineering Laboratory (NOEL) of Mediterranea University of Reggio Calabria (Italy), on a 1:15-scaled prototype of the structure. By using advanced optimization techniques, particularly Bayesian optimization, the models were refined, resulting in reliable predictions under diverse environmental conditions. The key outcomes of this study are outlined below:

- ANNs successfully captured the complex dynamics of offshore structures, proving their potential as a valuable tool for predicting dynamic responses.
- Incorporating techniques like Bayesian optimization contributed to improved model reliability, ensuring accurate dynamic response predictions for offshore platforms.
- Optimization techniques enhanced model performance, leading to reliable predictions under a range of operational scenarios and highlighting the potential of ANNs in managing offshore dynamics.
- Further investigation into data extremes, particularly under severe environmental conditions, may be useful. Such analyses could identify additional variables that may enhance model performance and offer valuable insights beyond average responses, potentially enabling predictions of other response variables.
- Ongoing fine-tuning of ANNs is essential for optimizing model architecture and hyperparameters, which will improve the model's predictive power and ensure robust performance in complex environments.
- Given that ANNs have shown effectiveness in this problem, investigating additional techniques, such as genetic algorithms, support vector machines, or hybrid AI models, which have already demonstrated value in similar applications, could further improve model performance in future studies.

- This research represents an important advancement in integrating AI with marine engineering, particularly in the deployment of dynamic response predictions for offshore platforms.

In summary, this study confirms the value of ANNs in addressing the challenges of offshore platform dynamics. However, ongoing refinements—such as focused dataset adjustments and the analysis of extremes—will be essential for improving predictive accuracy. With continued improvements, ANNs have the potential to play a critical role in the sustainable operation of marine infrastructure, representing a significant step forward for renewable energy platforms.

Author Contributions: Conceptualization, N.M., C.R., G.M., V.F. and F.A.; methodology, N.M. and G.M.; software, N.M.; validation, N.M.; formal analysis, N.M.; investigation, N.M.; resources, N.M., C.R., G.M., V.F. and F.A.; data curation, N.M., C.R. and V.F.; writing—original draft preparation, N.M.; writing—review and editing, N.M., C.R., V.F. and G.M.; visualization, N.M. and V.F.; supervision, G.M. and F.A. All authors have read and agreed to the published version of the manuscript.

Funding: This work was funded by the Next Generation EU—Italian NRRP, Mission 4, Component 2, Investment 1.5, call for the creation and strengthening of 'Innovation Ecosystems', building 'Territorial R&D Leaders' (Directorial Decree n. 2021/3277)—project Tech4You—Technologies for Climate Change Adaptation and Quality of Life Improvement, n. ECS0000009. This work reflects only the authors' views and opinions; neither the Ministry for University and Research nor the European Commission can be considered responsible for them.

Institutional Review Board Statement: Not applicable.

Informed Consent Statement: Not applicable.

Data Availability Statement: Data are not publicly available due to privacy restrictions. Data can be made available upon request to the authors.

Acknowledgments: The data used in this work have been obtained during "The Blue Growth Farm" project funded by the European Union's Horizon2020 research and innovation programme (Grant Agreement number 774426). The content of the work does not report the opinion of the European Commission and reflects only the views of the author(s), including errors or omissions. The European Commission is also not liable for any use that may be made of the information contained herein.

Conflicts of Interest: The authors declare no conflicts of interest. The funders had no role in the design of the study and in the writing of the manuscript.

References

1. Li, L.; Lin, J.; Wu, N.; Xie, S.; Meng, C.; Zheng, Y.; Wang, X.; Zhao, Y. Review and Outlook on the International Renewable Energy Development. *Energy Built Environ.* **2022**, *3*, 139–157. [CrossRef]
2. Akhtar, N.; Geyer, B.; Schrum, C. Larger Wind Turbines as a Solution to Reduce Environmental Impacts. *Sci. Rep.* **2024**, *14*, 6608. [CrossRef]
3. Billing, S.L.; Charalambides, G.; Tett, P.; Giordano, M.; Ruzzo, C.; Arena, F.; Santoro, A.; Lagasco, F.; Brizzi, G.; Collu, M. Combining Wind Power and Farmed Fish: Coastal Community Perceptions of Multi-Use Offshore Renewable Energy Installations in Europe. *Energy Res. Soc. Sci.* **2022**, *85*, 102421. [CrossRef]
4. Ruzzo, C.; Malara, G.; Collu, M.; Santoro, A.; Fiamma, V.; Scialò, A.; Lagasco, F.; Arena, F. Field Experiment on a Scaled Prototype of a Floating Multi-Purpose Offshore Platform: Dynamic Response Determination with Uncertainty Quantification. *Appl. Ocean Res.* **2022**, *129*, 103402. [CrossRef]
5. Gutiérrez-Romero, J.E.; García-Espinosa, J.; Serván-Camas, B.; Zamora-Parra, B. Non-Linear Dynamic Analysis of the Response of Moored Floating Structures. *Mar. Struct.* **2016**, *49*, 116–137. [CrossRef]
6. Ransley, E.J.; Greaves, D.; Raby, A.; Simmonds, D.; Hann, M. Survivability of Wave Energy Converters Using CFD. *Renew. Energy* **2017**, *109*, 235–247. [CrossRef]
7. Subbulakshmi, A.; Verma, M. Dynamic Response Analysis of a Semisubmersible Floating Offshore Wind Turbine Subjected to Mooring Line Failure Under Normal and Extreme Environmental Conditions. *Ocean. Eng.* **2024**, *304*, 117907. [CrossRef]
8. Michailides, C.; Gao, Z.; Moan, T. Experimental and Numerical Study of the Response of the Offshore Combined Wind/Wave Energy Concept SFC in Extreme Environmental Conditions. *Mar. Struct.* **2016**, *50*, 35–54. [CrossRef]

9. Castro-Santos, L.; Filgueira-Vizoso, A.; Carral-Couce, L.; Fraguela Formoso, J.Á. Economic Feasibility of Floating Offshore Wind Farms. *Energy* **2016**, *112*, 868–882. [CrossRef]
10. Drissi-Habti, M.; Neginhal, A.; Manepalli, S.; Carvelli, V. Fiber-Optic Sensors (FOS) for Smart High Voltage Composite Cables—Numerical Simulation of Multi-Parameter Bending Effects Generated by Irregular Seabed Topography. *Sensors* **2022**, *22*, 7899. [CrossRef]
11. Drissi-Habti, M.; El Assami, Y.; Raman, V. Multiscale Toughening of Composites with Carbon Nanotubes—Continuous Multiscale Reinforcement New Concept. *J. Compos. Sci.* **2021**, *5*, 135. [CrossRef]
12. Zhang, Q.; Drissi-Habti, M. Electric Cable Insulator Damage Monitoring by Lasso Regression. *Machines* **2024**, *12*, 50. [CrossRef]
13. Normandia Lourenço, L.F.; Louni, A.; Damm, G.; Netto, M.; Drissi-Habti, M.; Grillo, S.; Sguarezi Filho, A.J.; Meegahapola, L. A Review on Multi-Terminal High Voltage Direct Current Networks for Wind Power Integration. *Energies* **2022**, *15*, 9016. [CrossRef]
14. Panda, J.P. Machine Learning for Naval Architecture, Ocean and Marine Engineering. *J. Mar. Sci. Technol.* **2023**, *28*, 1–26. [CrossRef]
15. Pezeshki, H.; Adeli, H.; Pavlou, D.; Siriwardane, S.C. State of the Art in Structural Health Monitoring of Offshore and Marine Structures. *Proc. Inst. Civ. Eng.—Marit. Eng.* **2023**, *176*, 89–108. [CrossRef]
16. Li, D.; Jiang, M.-R.; Li, M.-W.; Hong, W.-C.; Xu, R.-Z. A Floating Offshore Platform Motion Forecasting Approach Based on EEMD Hybrid ConvLSTM and Chaotic Quantum ALO. *Appl. Soft Comput.* **2023**, *144*, 110487. [CrossRef]
17. Chen, Y.; Yuan, L.; Qin, L.; Zhang, N.; Li, L.; Wu, K.; Zhou, Z. A Forecasting Model with Hybrid Bidirectional Long Short-Term Memory for Mooring Line Responses of Semi-Submersible Offshore Platforms. *Appl. Ocean Res.* **2024**, *150*, 104145. [CrossRef]
18. Jiang, H.; Wang, H.; Vaz, M.A.; Bai, X. Research on Dynamic Response Prediction of Semi-Submersible Wind Turbine Platform in Real Sea Test Model Based on Machine Learning. *Appl. Ocean Res.* **2024**, *142*, 103808. [CrossRef]
19. Das, P.; Mashiata, M.; Iglesias, G. Big Data Meets Big Wind: A Scientometric Review of Machine Learning Approaches in Offshore Wind Energy. *Energy AI* **2024**, *18*, 100418. [CrossRef]
20. Ahmad, I.; M'zoughi, F.; Aboutalebi, P.; Garrido, I.; Garrido, A.J. Fuzzy Logic Control of an Artificial Neural Network-Based Floating Offshore Wind Turbine Model Integrated with Four Oscillating Water Columns. *Ocean. Eng.* **2023**, *269*, 113578. [CrossRef]
21. Cai, Z.; Zhang, B.; Yu, X. Neural Network Delayed Control of an Idealized Offshore Steel Jacket Platform. In Proceedings of the Eighth International Conference on Intelligent Control and Information Processing (ICICIP), Hangzhou, China, 3–5 November 2017; pp. 282–286. [CrossRef]
22. Cotrim, L.P.; Barreira, R.A.; Santos, I.H.F.; Gomi, E.S.; Costa, A.H.R.; Tannuri, E.A. Neural Network Meta-Models for FPSO Motion Prediction from Environmental Data with Different Platform Loads. *IEEE Access* **2022**, *10*, 86558–86577. [CrossRef]
23. Abaei, M.M.; Abbassi, R.; Garaniya, V.; Chai, S.; Khan, F. Reliability Assessment of Marine Floating Structures Using Bayesian Network. *Appl. Ocean Res.* **2018**, *76*, 51–60. [CrossRef]
24. Mahdavi-Meymand, A.; Sulisz, W. Development of Pyramid Neural Networks for Prediction of Significant Wave Height for Renewable Energy Farms. *Appl. Energy* **2024**, *362*, 123009. [CrossRef]
25. Bak, C.; Zahle, F.; Bitsche, R.; Kim, T.; Yde, A.; Henriksen, L.C.; Hansen, M.H.; Blasques, J.P.A.A.; Gaunaa, M.; Natarajan, A. The DTU 10-MW Reference Wind Turbine. *Sound/Vis. Prod. (Digit.)* **2013**. Available online: https://orbit.dtu.dk/en/publications/the-dtu-10-mw-reference-wind-turbine (accessed on 4 November 2024).
26. Malara, G.; Arena, F. Response of U-Oscillating Water Column Arrays: Semi-Analytical Approach and Numerical Results. *Renew. Energy* **2019**, *138*, 738–748. [CrossRef]
27. Ruzzo, C.; Fiamma, V.; Scialò, A.; Arena, F.; Santoro, A.; Muggiasca, S.; Taruffi, F.; Di Carlo, S.; Larrea, I.; Corvaglia, P.A.; et al. Field Experimental Campaign on a Multi-Purpose Floating Structure: Set-up Description. In *Trends in Renewable Energies Offshore—Proceedings of the 5th International Conference on Renewable Energies Offshore, Lisbon, Portugal, 8–10 November 2022*; RENEW; CRC Press: Boca Raton, FL, USA, 2022; pp. 817–825. [CrossRef]
28. Boccotti, P. Space–Time Theory of Sea States. In *Wave Mechanics and Wave Loads on Marine Structures*; Elsevier: Amsterdam, The Netherlands, 2015; pp. 115–143. [CrossRef]
29. Boccotti, P.; Arena, F.; Fiamma, V.; Romolo, A.; Barbaro, G. Estimation of Mean Spectral Directions in Random Seas. *Ocean Eng.* **2011**, *38*, 509–518. [CrossRef]
30. Joseph, V.R. Optimal Ratio for Data Splitting. *Stat. Anal. Data Min. ASA Data Sci. J.* **2022**, *15*, 531–538. [CrossRef]
31. TensorFlow Developers. TensorFlow (v2.18.0). *Zenodo*. 2024. Available online: https://zenodo.org/records/13989084 (accessed on 4 November 2024).
32. Li, L.; Jamieson, K.G.; DeSalvo, G.; Rostamizadeh, A.; Talwalkar, A. Hyperband: A Novel Bandit-Based Approach to Hyperparameter Optimization. *J. Mach. Learn. Res.* **2018**, *18*, 1–52. [CrossRef]
33. Feurer, M.; Hutter, F. Hyperparameter Optimization. In *Automated Machine Learning*; Hutter, F., Kotthoff, L., Vanschoren, J., Eds.; Springer: Cham, Switzerland, 2019; pp. 3–33. [CrossRef]
34. Louppe, G.; Wehenkel, L.; Sutera, A.; Geurts, P. Understanding Variable Importances in Forests of Randomized Trees. In Proceedings of the Advances in Neural Information Processing Systems 26 (NIPS 2013), Lake Tahoe, NV, USA, 5–8 December 2013; pp. 431–439.
35. Fisher, A.; Rudin, C.; Dominici, F. All Models Are Wrong, but Many Are Useful: Learning a Variable's Importance by Studying an Entire Class of Prediction Models Simultaneously. *J. Mach. Learn. Res.* **2019**, *20*, 1–81.

36. Breiman, L. Random Forests. *Mach. Learn.* **2001**, *45*, 5–32. [CrossRef]
37. Pedregosa, F.; Varoquaux, G.; Gramfort, A.; Michel, V.; Thirion, B.; Grisel, O.; Duchesnay, E. Scikit-Learn: Machine Learning in Python. *J. Mach. Learn. Res.* **2011**, *12*, 2825–2830. [CrossRef]